Flexible and Printed Electronics

An acrylate resin/perfluoropolyether film with enhanced hydrophobicity and lowered adhesion surface for precision printed electronics

To cite this article: Hui Xu *et al* 2025 *Flex. Print. Electron.* **10** 045005

Flexible and Printed Electronics

OPEN ACCESS

RECEIVED
18 March 2025

REVISED
26 August 2025

ACCEPTED FOR PUBLICATION
30 September 2025

PUBLISHED
3 November 2025

PAPER

An acrylate resin/perfluoropolyether film with enhanced hydrophobicity and lowered adhesion surface for precision printed electronics

Hui Xu[1,2,3], Ke Shui[2,3], Xin Li[4], Subin Jiang[5], Qingyuan Li[4], Ni Yin[2], Zhiyun Li[6], Yabin Zhang[6], Jian Lin[2,3,5,*], Qi Chen[2], Song Qiu[4], Fengqi Guo[1,*] and Chang-Qi Ma[2,3,5,*]

[1] Henan Institute of Advanced Technology, Zhengzhou University, 97 Wenhua Road, Zhengzhou 450000, People's Republic of China
[2] i-Lab, Suzhou Institute of Nano-Tech and Nano-Bionics, Chinese Academy of Sciences, SEID, SIP, 215123 Suzhou, People's Republic of China
[3] Printable Electronics Research Center, Suzhou Institute of Nano-Tech and Nano-Bionics, Chinese Academy of Sciences, SEID, SIP, 215123 Suzhou, People's Republic of China
[4] Division of Advanced Materials, Suzhou Institute of Nano-Tech and Nano-Bionics, Chinese Academy of Sciences, Suzhou 215123, People's Republic of China
[5] Engineering Center of Precision Printing Manufacturing, Guangdong Institute of Semiconductor Micro-Nano Manufacturing Technology, Kejiao Road No. 1, Shishan Town, 528225 Foshan, People's Republic of China
[6] Vacuum Interconnected Nanotech Workstation, Suzhou Institute of Nano-Tech and Nano-Bionics, Chinese Academy of Sciences (CAS), 398 Ruoshui Road, SEID, SIP, Suzhou 215123, People's Republic of China
[*] Authors to whom any correspondence should be addressed.

E-mail: jlin2010@sinano.ac.cn, fqguo@zzu.edu.cn and cqma2011@sinano.ac.cn

Keywords: sliding angle, ultraviolet light response, spontaneous patterning, heterogenous wettability pattern, printed circuit

Supplementary material for this article is available online

Abstract

Spontaneously patterned circuits are regarded as one of the most promising green manufacturing methods that are non-lithographic and mold-free, attracting increasing attention. Liquid-mimicking surfaces allow polar or non-polar liquids to slide easily on slightly inclined modified surfaces without residue, achieving liquid repulsion and self-cleaning functions. Combining the advantages of this sliding property with specific patterned physicochemical characteristics is expected to further enhance printing resolution. In this manuscript, we developed a heterogeneous composite film consisting of a UV-sensitive (2-nitro-1,4-phenylene) bis(methylene) diacrylate resin film (referred to as NBE) overlaid with a layer of hydrophobic perfluoropolyether (referred to as 507 A). The tunable surface property of the NBE resin film under UV light ($\lambda = 254$ nm) irradiation enables the hydrophobic surface (with a water contact angle, WCA of 112°) of the composite film to a hydrophilic surface (with a WCA of 4°), allowing the formation of patterned wettability surface after light exposure. More importantly, the highly hydrophobic perfluoropolyether surface shows a low adhesive surface, which enables a cleaner surface in the hydrophobic area during printing. Angle-resolved x-ray photoelectron spectroscopy and atomic force microscopy tests revealed the differences in surface morphology and elemental distribution of the composite film before and after UV light exposure. In combination with a photomask, fine circuit structures with minimal line width/space of 5/5 μm were successfully achieved. The printed circuit was used for carbon nanotube-based thin film transistors, which displayed charge carrier mobilities of 4.51 ± 1.63 $cm^2 \cdot s^{-1} \cdot V^{-1}$, demonstrating the practicality of this precision printing technique.

1. Introduction

Printed electronics is a new technology that uses traditional printing (or coating) to manufacture electronic components and products [1]. Printed electronics can be applied to prepare flexible keyboards, photodetectors, sensors, electronic skins etc [2, 3]., suitable for the fast development of wearable and ultra-thin electronic devices, and have attracted much attention in the past few years. The production of printed electronic components requires high precision in terms of product resolution, integration, and information capacity. Conventional printing techniques, such as inkjet printing [4], gravure printing [5], screen printing [6], and blade coating [7] have been able to achieve resolutions mostly concentrated in the range of tens to hundreds of micrometers. The issue of low resolution has limited the application scenarios of printed electronics processes.

Recently, spontaneously patterned circuits using heterogeneous wettability patterns to guide ink droplet motion have emerged as one of the most promising green manufacturing methods offering non-lithographic and mold-free approach. The key to the heterogeneous wettability patterns for printing conductive circuits was the induction of constructing surface energy pattern regions with high contrast [8, 9], which allowed for the precise control of ink spreading and flow on the substrate. When ink drop is deposited on pre-patterned wettability gradient areas, it will be driven from hydrophobic regions to hydrophilic regions due to the different surface energies of the substrate [10], and the ink will limited on the patterned area forming patterned circuit preprepared. With these, a combination of surface energy confinement effect and printing process that utilizes a pre-patterned hydrophilic-hydrophobic surface to enhance printing resolution to the sub-micrometer level have been developed in the last few years [11], and are recognized as one of the most promising green manufacturing methods that are non-lithographic and mold-free, attracting increasing attention.

The preparation of heterogeneous wettability patterns includes direct printing preparation, plasma treatment of hydrophobic surfaces, ultraviolet light irradiation of hydrophobic surfaces, etc. Feng *et al* used inkjet printing to deposit ink containing water-soluble dyes and high-boiling-point alcohols on the surface of the HC film. The ink can wet the film and increase the surface hydrophilicity. The NaOH aqueous solution can selectively penetrate into the ink-painted areas. After etching, wettability-differential patterns are formed, with a resolution of up to 200 μm [12]. However, there are still certain limitations on the resolution in the preparation by direct printing. In terms of surface energy gradient-guided inkjet printing technology, Naderi *et al* proposed a sequential printing and drying method. Without the need for surface modification, this method can form micro—patterns such as straight lines and triangles on hydrophobic surfaces like Teflon-AF [13]. However, this method has some limitations. For example, it requires multiple rounds of printing and drying, has high requirements for parameter control, and has limited precision and large errors when preparing complex patterns. Similarly, Matthew and others adapted the stacked coin strategy by heating the substrate. By accurately controlling the relationship between the deposition time and evaporation time of droplets, they successfully achieved continuous line inkjet printing on hydrophobic surfaces without pretreatment, providing a new method for printing on hydrophobic surfaces [14]. But in terms of technology, this method is restricted by problems such as easy nozzle clogging, high temperature requirements, and insufficient mechanical strength. In the future, further exploration is needed in equipment optimization, material adaptation, and theoretical model improvement.

Besides direct printing preparation, the surface can also be modified by using plasma [15, 16], which has the advantages of not requiring complicated pretreatment steps and being able to construct hydrophilic and hydrophobic patterns in one step. Pierre *et al* deposited a hydrophobic fluorosilane-based monolayer on an oxygen plasma-treated substrate. They then used a stainless steel mask to selectively apply plasma treatment, creating a patterned surface and ultimately achieved highly homogeneous printing of metal source-drain arrays as well as semiconductor active layer arrays using a blade-coating method [17]. Although this method simplifies the process, the high cost of plasma treatment equipment and the stringent requirements for the operating environment limit its large-scale application. In addition, the channel length of the transistors fabricated in this literature is 20 μm. By comparison, there is still room for improvement in high-resolution fabrication capabilities. In addition, UV irradiation can also be used for surface modification to construct heterogeneous wettability patterns [18]. Liu *et al* previously reported a spontaneous patterning technique based on parallel vacuum ultraviolet irradiation, which was utilized for the uniform integration of complex, high-resolution electronic circuits [19, 20]. By irradiated with a parallel light source of 172 nm, the hydrophobic polymer surface of parylene-C was transformed selectively into highly wettable areas by breaking the chemical bonds. This process resulted in the generation of highly uniform wettability arrays on the polymer surface and successfully enabled the large-scale fabrication of short-channel organic thin-film transistors

with widths as low as 1 μm on PET substrates. UV irradiation for generating heterogeneous wettability patterns is known for its simplicity of operation, short processing time, efficiency [21], and controllability in terms of time and space [22], and can be carried out at room temperature [23]. However, the parallel light source of 172 nm is costly, has limited accessibility, and suffers from a short lifespan.

To avoid the use of 172 nm VUV light, we recently developed a light-sensitive NBE-acrylate resin for the preparation of a diverse wetting surface. This approach was developed based on the work of Rossegger *et al*, who demonstrated that hydrophobic cross-linked NBE-acrylate resin surfaces can be converted to hydrophilic surface under 254 nm UV light irradiation [24]. Using an optimized silver ink formulation, circuits with a line width/space (L/S) of 10/10 μm were fabricated by blade coating [11]. However, as demonstrated later in this study, the high sliding angle of silver ink droplets on the hydrophobic NBE resin surface impedes ink droplet movement, hindering the migration and separation of conductive ink and limiting further resolution improvement.

In this work, we developed a composite film by overlaying a perfluoropolyether layer on top of an NBE resin film, creating a dual-layer composite film. The perfluoropolyether layer showed a hydrophobic surface with a high water contact angle (WCA) of 113° with low water rolling angle of 47°. Interestingly, although the perfluoropolyether layer is deposited on top of NBE, the underlying NBE layer undergoes photodecomposition under 254 nm ultraviolet irradiation, yielding a hydrophilic surface with a WCA of 4°. By using a photomask, the exposed area becomes hydrophilic while the non-exposed area remains hydrophobic with a low sliding angle, allowing for the precise manufacturing of fine structures through printing processes. This has led to a further enhancement in resolution compared to single-layer NBE films. The detailed hydrophobic–hydrophilic conversion of the composite film as well as the preparation of the carbon nanotube (CNT) based transistors will be discussed in detailed in this study.

2. Results and discussion

2.1. Preparation of composite films and UV-induced surface energy regulation

Our previous works have demonstrated that the hydrophobic acrylate-NBE resin surface can be converted into hydrophilic surface under 254 nm UV light irradiation and printed circuits with L/S of 10/10 μm were successfully fabricated. Further attempts to increase the resolution of the printed circuit were not successful, which was ascribed to the failure of separating ink film by the hydrophobic regions. This is likely due to the high adhesive interface between hydrophobic NBE surface and silver ink (*vide infra*). To reduce the adhesion of the ink droplet on NBE surface, a commercially available perfluoropolyether (referred to as 507 A) was selected as the top covering layer of the NBE film. Figure 1(a) shows the preparation process of the composite film and the following printing of the electric circuits. Prior to 254 nm irradiation, the cross-linked PEB film was spin-coated with 507 A. Figures 1(b) and (c) show the static (WCA, droplet size 2 μl) and water sliding angles (WSA, droplet size 8 μl, measurement limit 90°) of the pristine 507 A and NBE/507 A films, where the 507 A layers were spin-coated at different spin speeds. The static WCA of the 507 A film on glass decreases slightly from 115° to 105° with the increase of spin speed, whereas the WSA increases from 20° to 90° (the upper limit). This indicates that 507 A has hydrophobic properties with low adhesion to water droplets, and the thicker 507 A layer enhances hydrophobicity while further reducing adhesion. Similar to the pristine 507 A film, the static WCA of the NBE/507 A composite films decreases slightly from 114° to 108° with the increase of spin speed, while the WSAs were measured to be 39° and 47° when the 507 A layer was spin-coated at 1000 and 2000 rpm and then increased to 90° (the maximum value for WSA measurement) when the 507 A spin speed is higher than 3000 rpm, suggesting that the interfacial adhesion between NBE/507 A increases significantly when 507 A layer is too thin. In contrast, the pristine NBE film shows static WCA and WSA of 102° and 90°, respectively, indicating a hydrophobic but high adhesive surface to water droplet. Therefore, the hydrophobic 507 A film should be able to reduce the adhesion to the ink droplet, however one should keep enough thickness for the 507 A layer. For our purposes, we kept using 507 A layer coated at 2000 rpm for further studies. Meanwhile, we prepared NBE/507 A composite films on PET. Although the conditions were not fully optimized, we tested the WCA of the films after bending and found that the excellent hydrophobic properties were still maintained after 20 000 bending cycles, (see figure S3 in supporting information) indicating good stability and potential for application in flexible electronic devices.

To confirm whether UV light irradiation can alter the surface properties of the NBE/507 A composite film, composite NBE/507 A films (prepared at 2000 rpm) were irradiated with 254 nm UV light (25 mW cm^{-2}), and their WCAs were measured. The results are shown in figure 1(d). For comparison, the changes of WCA on 507 A and NBE films were also measured. As seen here, upon UV light illumination, the WCA on NBE film decreased gradually from 102° to 6° with the increase of UV illumination time, similar to our previous report. In contrast, the

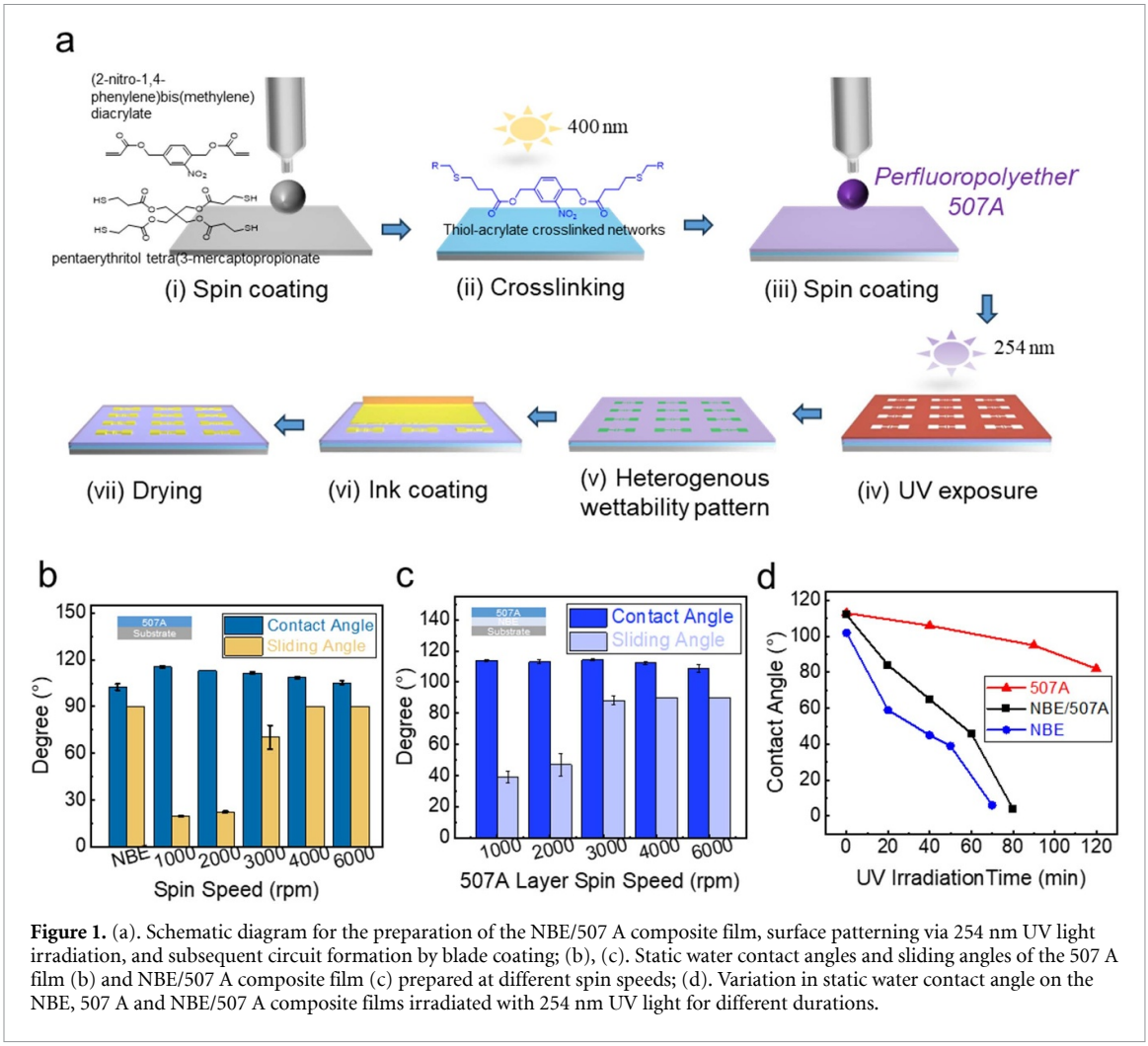

Figure 1. (a). Schematic diagram for the preparation of the NBE/507 A composite film, surface patterning via 254 nm UV light irradiation, and subsequent circuit formation by blade coating; (b), (c). Static water contact angles and sliding angles of the 507 A film (b) and NBE/507 A composite film (c) prepared at different spin speeds; (d). Variation in static water contact angle on the NBE, 507 A and NBE/507 A composite films irradiated with 254 nm UV light for different durations.

WCA on 507 A surface decreases only slightly from 113° to 82° even with UV irradiation for 120 min, suggesting that the 507 A surface energy cannot be altered to hydrophilic by simple 254 nm UV irradiation. To help us understand the mechanism of hydrophilic-hydrophobic transformation in composite films, we also tested the atomic force microscopy (AFM) images of the 507 A film before and after irradiation with 254 nm ultraviolet light (see figure S4 in the supporting information) and found that the surface roughness increased. Although we cannot fully understand the changes in 507 A under 254 nm UV irradiation, the results of contact angle and AFM tests indicate that it remains relatively stable under 254 nm UV irradiation. Additionally, the roughness of the composite film after light irradiation is reduced compared to both the 507 A film and the NBE film. Surprisingly, the NBE/507 A composite film exhibited a significant decrease in WCA under UV light irradiation. The WCA decreased from 112° for the pristine film decreases gradually to 4° when the film was irradiated for 80 min, demonstrating that 254 nm UV light can convert the hydrophobic NBE/507 A surface to an hydrophilic surface, which would be ideal for the construction of heterogeneous surface for printed electronics.

2.2. Morphology and chemical composition evolution of the NBE/507 A composite films under UV-light illumination

To better understand the mechanism of surface energy alternation, surface morphology and chemical composition of the NBE/507 A composite films were measured by AFM and angle-resolved x-ray photoelectron spectroscopy (ARXPS). Figures 2(a) and (b) depict the high-resolution ARXPS results of F 1s, N 1s, and S 2p of the NBE/507 A films before (figure 2(a)) and after (b) UV irradiation. For the NBE/507 A composite film, intensive F 1s peaks were measured both before and after UV irradiation, demonstrating the successful deposition of 507 A on NBE and no significant decomposition of 507 A under UV irradiation. Very weak N 1s signals were measured for the composite film before UV irradiation, whereas increased N 1s peak at 400 eV was measured after UV exposure. This can be ascribed to the formation of nitroso moieties in acrylate-NBE after UV irradiation [11, 25]. There were two

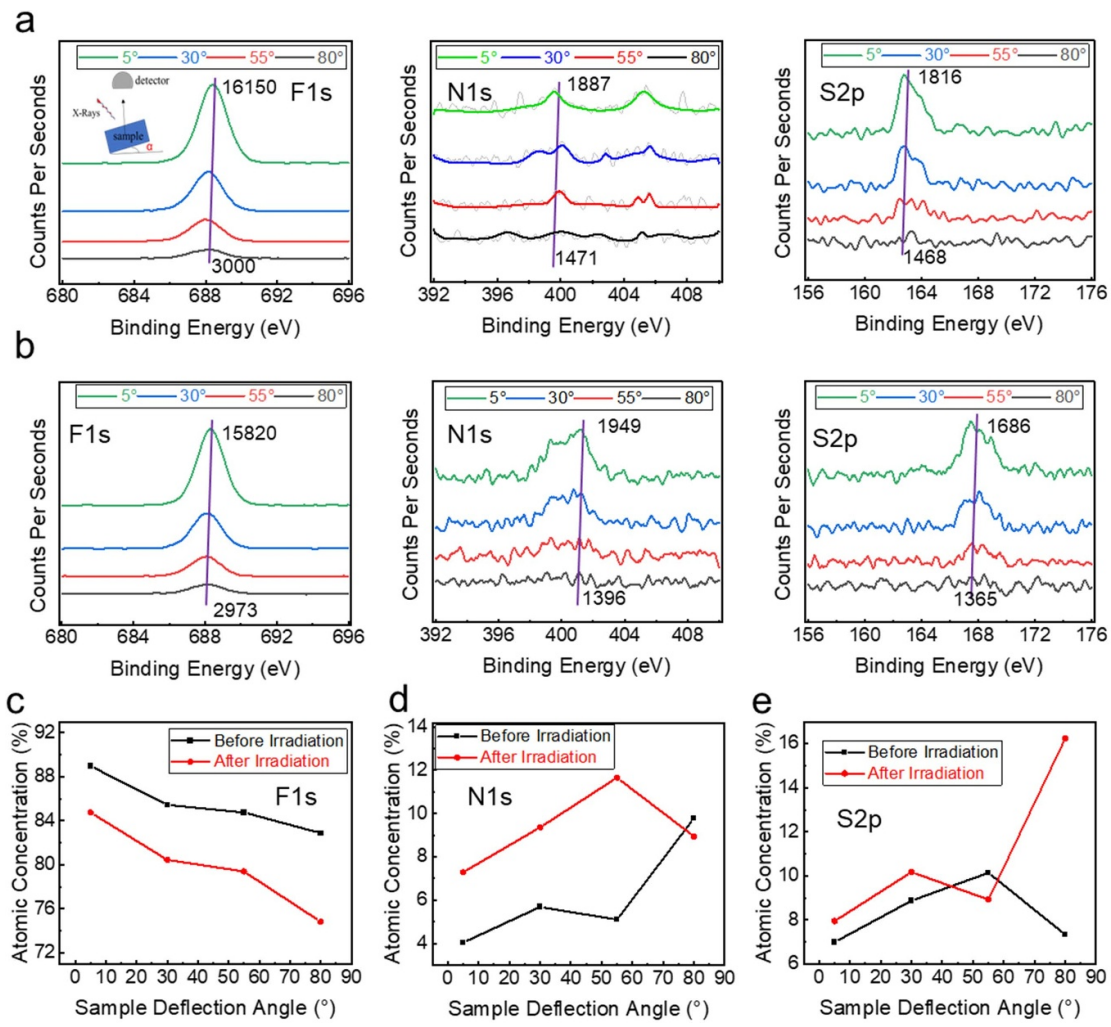

Figure 2. High-resolution ARXPS of F 1s, N 1s, S 2p of the NBE/507 A composite thin-film before (a) and after (b) UV irradiation.; (c), (d), (e)) Variation of F (c), N (d), and S (e) elemental content of NBE/507 A film with sample tilted angle before and after UV irradiation.

peaks at around 400 eV and 405.5 eV for nitrogen before irradiation, which corresponded to nitro groups (–NO_2, 405.5 eV) in the NBE layer and the C–N bond in the MD700 resin [26]. After irradiation, the nitro groups are converted to nitroso moieties [9]. Most interestingly, the S 2p signal for the composite film before UV irradiation was measured to be 163 eV, corresponding to C–S–C bonds [9] of the NBE resin after cross-linking. This signal was converted to 168 eV after UV irradiation, demonstrating the formation of –SO_3 bonds [27, 28]. This clearly confirmed the conversion of C–S–C bonds to –SO_3 bonds under light illumination, which explains the formation of hydrophilic surface. Moreover, the N 1s signal after irradiation was stronger than that before irradiation. Since it is known that nitrogen (N) and sulfur (S) only came from the NBE resin, after irradiation, the components belonging to NBE moved to a more surface position.

Under the same deflection angle of the sample, the measured F 1s, N 1s and S 2p were normalized to the peak areas after deducting the back bottom to obtain the relative contents of the atoms. The relative contents of F 1s, N 1s and S 2p detected at different twist angles are shown in figures 2(c)–(e). It can be clearly seen that the content of F decreases after illumination, whereas the N 1s and S 2p relative contents increased after UV irradiation. Together with the facts that higher N 1s and S 2p signals were measured with larger sample twisting angle, one can conclude the floating up of the hydrophilic NBE components and the sinking of 507 A upon UV irradiation.

From a qualitative perspective, there were hydrophilic substances formed after the photolysis of NBE on the surface of the composite film after irradiation, which further corroborated that more NBE from the bottom layer moved to the surface layer after irradiation and became hydrophilic under ultraviolet irradiation.

Figure 3(a) depicts the AFM height images of the NBEand NBE/507 A films before and after UV irradiation. It can be observed that the pristine NBE film showed a homogenous surface with a root mean square roughness (Rq) of 0.34 nm, whereas the

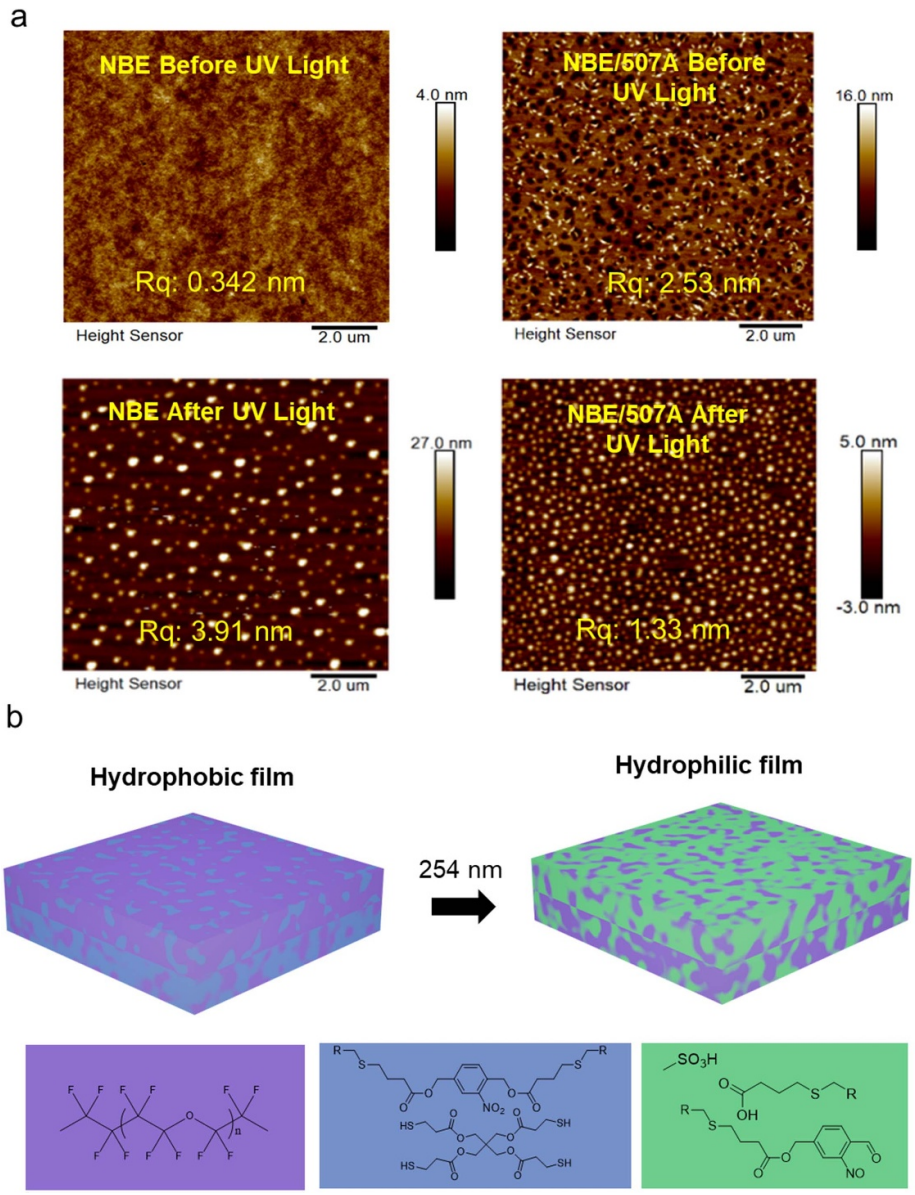

Figure 3. (a) AFM height images of NBE and NBE/507 A films before and after UV irradiation; (b) schematic diagram illustrating the chemical and morphology change of the NBE/507 A film after UV irradiation.

UV-irradiated film displayed a rougher surface with an Rq of 3.91 nm, where large aggregates, ranging in diameter from tens to hundreds of nanometers, can be clearly identified. The change of surface morphology of the NBE film can be ascribed to the photon decomposition of NBE molecules, yielding much hydrophilic groups, such as carboxylic acids and aldehydes etc. (see figure S2 in supporting information) [11, 29]. After the deposition of 507 A, the NBE/507 A composite film showed a rough surface with voids and particles in hundreds of nanometers scale, yielding an Rq of 2.53 nm. Detailed mechanism for the formation of the rough surface is not clear yet, the voids can be ascribed to the washing effect of solvent of 507 A during the spin coating, while the particles are proposed to be the aggregates of 507 A owning to the poor wettability of 507 A on NBE surface. Larger particles were measured for the NBE/507 A film after UV irradiation. Together with the formation of particles of NBE film, the measured morphology of the NBE/507 A film originated from the photodecomposition of NBE resin under UV light illumination. This is in good accordance with the significantly decreased WCA of the UV-treated composited film. We observed that the roughness of the composite film increased to some extent after light irradiation, although the roughness of the composite film was lower than that of the UV-irradiated NBE film. This might have caused certain adverse effects on the uniformity of devices and fine lines as well as interfacial charge transport. While it is difficult to quantitatively analyze the impact on uniformity, the measured carrier mobility of the fabricated devices reached 2.21–7.80 $cm^2 \cdot V^{-1} \cdot s^{-1}$, indicating no obvious negative influence.

With the XPS and AFM results, a mechanism for the conversion of hydrophobic surface of NBE/507 A composite film to the hydrophilic surface is proposed in figure 3(b). Under 254 nm UV irradiation, the underlying hydrophobic NBE layer decomposed and moved toward to the surface, which drag the hydrophobic 507 A to the underneath. Most importantly, the hydrophilic groups of carbonic acid (–COOH), aldehyde (–CHO), and sulfonic acid ($–SO_3$) groups facing to the thin film surface, leading to a hydrophilic property of the final film.

2.3. Optimization of ink formulation for high-resolution printed circuit

The small water sliding angle would help in driving the ink droplet to move to hydrophilic area, which is believed to be helpful in achieving high-resolution printed circuits. Even though ink formation needs to be well optimized to achieve this goal. We therefor measured the WCA and WSA of water and diethylene glycol monomethyl ester (DGME) mixtures which are the most commonly used solvent for dispersing silver nanoparticles. Figures 4(a) and (b) shows the variation of WCA and WSA with the content of the solvent mixture. As seen here, with the decrease of water content, the WCA on hydrophobic surface decreases gradually from 113° (for pure water) to 77° (for pure DGME), whereas the WCA keeps constant of $<10°$ on the UV-treated surface, indicating that all solvent mixtures are highly wettable on the hydrophilic surface. Relatively high WSA of ∼46° was measured for the solvents with DGME less than 50% (figure 4(b)). Further increase of DGME content decrease WSA to 37° for the pure DGME solvent. Nevertheless, the WCA differences of the solvent on the hydrophobic and hydrophilic regions are greater than 50°, which ensures a sufficient driving force for the surface dewetting process.

We then prepared fine electric circuits on the heterogenous wettability patterns surface. Figure 4(c) shows the printed fine circuits with L/S of 20/100 μm, 20/50 μm, 10/50 μm, 5/100 μm, 5/20 μm, 5/5 μm. The finest lines L/S of 5/5 μm were successfully fabricated, confirming that a small sliding angle helps to improve the printing resolution. Interestingly, during the fabrication of silver electrodes with a channel width of 5 μm, although a high contact angle difference was measured for water on different surfaces, no silver trace was left on the patterned surface when water-based Ag ink was used (figure 4(d)). This demonstrated that a poor wettability of ink droplet on surface will leads to the difficulties in ink remaining during coating process. In other words, one cannot simply rely on the wettability difference of the patterned surface for preparing the printed circuits. The introduction of DGME in the ink decrease the surface tension, that enables the deposition of Ag nanoparticles. Figure 5(d) shows the successful preparation of electrode with a designed gap of 5 μm using Ag inks with water: DGME ratios of 1:2 and 1:5, which yields a measured gap of 18 μm and 7 μm respectively. Further increase the content of DGME in the ink yield no separation of the gap, which can be due to the insufficient driving force for ink separation owing to its low surface tension. We have counted the relationship between the actual channel widths of the fabricated silver electrode samples and the inks, as shown in figure 5(e)–(g). It indicates that as the content of DGME increases, the actual channel widths change from large to small and are getting closer and closer to the designed channel widths. Based on the ink with a DGME of 1:5, electrodes with a channel width of 5 μm can be fabricated. Inks with water: DGME ratios of 1:6 and 0:1 can respectively fabricate electrodes with a channel width of 10 μm and silver electrodes with a channel width of 20 μm The reason for the successful fabrication of fine circuits may be that the surface tension and surface energy of the solid surface have reached a balance. These results indicate that the model design for the correlation between substrate patterns and inks can scientifically guide the printing process. We plan to investigate graphic structures with different duty cycles and their final patterns, thereby establishing a quantitative model for the influence of ink rheology on the final pattern. Relevant results will be published in a separate paper.

2.4. Transistors based on printed silver electrodes

We then fabricated thin film transistors (TFTs) based on the electrodes with different channel widths. Figure 5(a) shows the TFT structure, where CNTs deposited on 50 nm SiO_x were used as the semiconductor layer. Figure 5(b) shows the optical microscope images of the printed electrodes on glass with channel widths of 30 -100 μm. Limited by the mask we used, a large-area electrode array of 1.5×2.5 cm^2 was successfully prepared (see figure S5 in supporting information). Although the printing process was not fully optimized, only a few defects were observed in the effective area of 4 cm^2. It is worth noting that thermal annealing was performed on the printed electrode to enhance the conductivity. Figure 5(c) shows the I–V characteristics of the electrodes after thermal annealing at a distance of around 333 μm, with which a conductivity of 10^4 S $\cdot$ m^{-1} was measured for the annealed Ag films (figure S7 in supporting information). In contrast, a low current of less than 10^{-12} A was measured for the electrodes on both sides of the broken channel, indicating that a clean channel was prepared by this method.

TFT transistors were fabricated via a solution deposition process. Figures 5(d)–(f) present the output and transfer curves of transistors with varying channel lengths. Key performance metrics—including current on/off ratio (I_{ON}/I_{OFF}), carrier mobility (μ), and threshold voltage (V_{TH})—were derived from positive sweep data and are directly

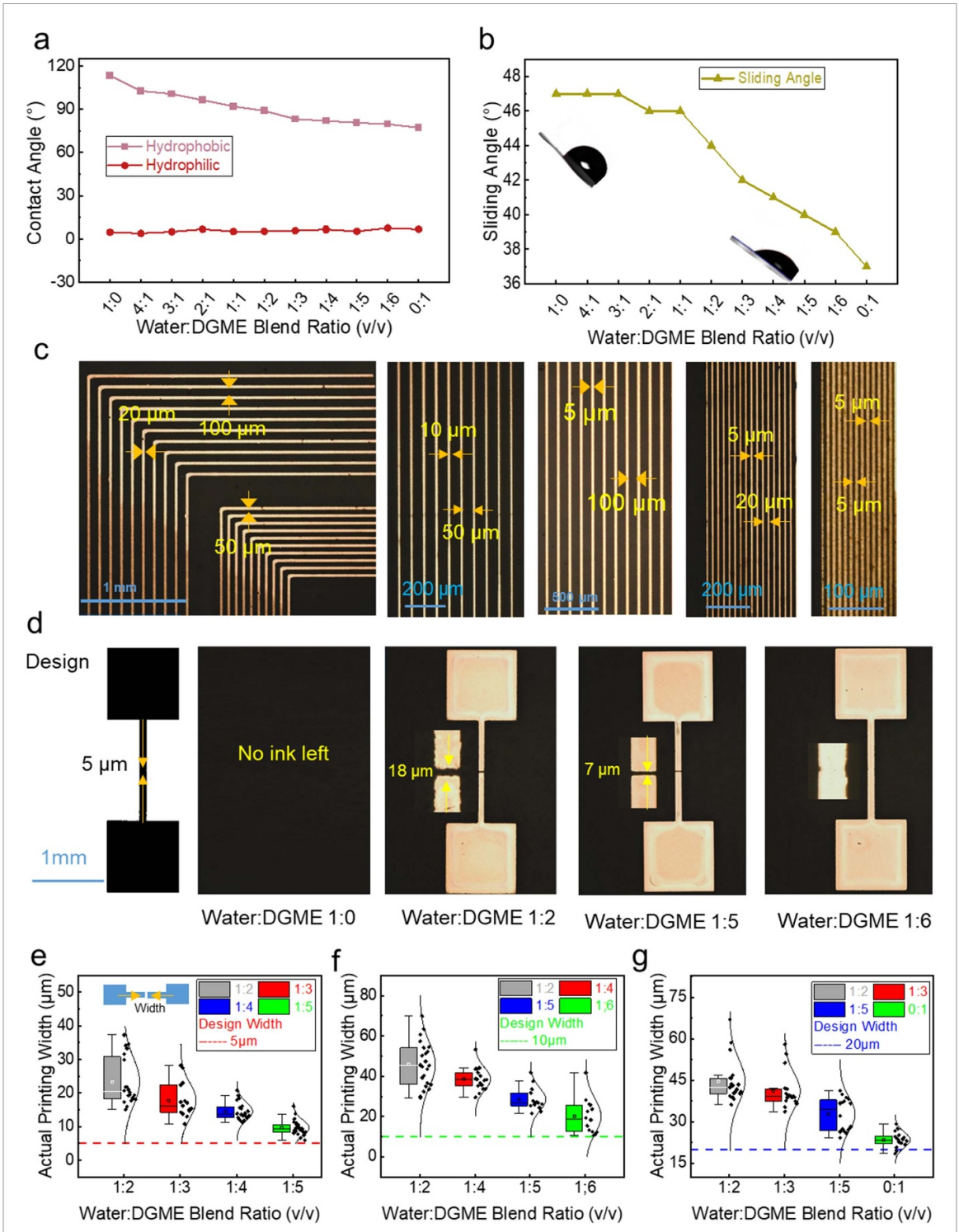

Figure 4. (a) Contact angles of the water:diethylene glycol monomethyl ester (DGME) on the hydrophobic (the pristine) and hydrophilic (UV-treated) surface, the blend ratio is in volume; (b) sliding angles of DGME on the hydrophobic surface; (c) sample of the fine circuits with line width of with L/S of 20/100 μm、20/50 μm、10/50 μm、5/100 μm、5/20 μm、5/5 μm; (d) surface morphology of the dried film coated from different silver inks, the designed pattern of the photomask (width = 5 μm) is shown on the left; ((e)–(g)) actual channel widths of electrodes prepared by scraping with different inks (e) design width = 5 μm, (f) design width = 10 μm, (g) design width = 20 μm.

labeled in the figures. Notably, all devices exhibited high I_{ON}/I_{OFF} ratios on the order of 10^4 and the devices also demonstrate excellent carrier mobility, which is 4.51 $\pm$ 1.63 $cm^2 \cdot V^{-1} \cdot s^{-1}$. The mobilities from the positive sweep and negative sweep are shown in table 1 and figure S8 of the Supporting Information. We calculated the average values of the mobilities from both the positive sweep and negative sweep after excluding one maximum and one minimum value. The results indicate that the mobility from the positive sweep is 4.51 $\pm$ 1.63 $cm^2 \cdot V^{-1} \cdot s^{-1}$, and the mobility from the negative sweep is 4.28 $\pm$ 1.31 $cm^2 \cdot V^{-1} \cdot s^{-1}$. It can be seen that the mobilities obtained from the

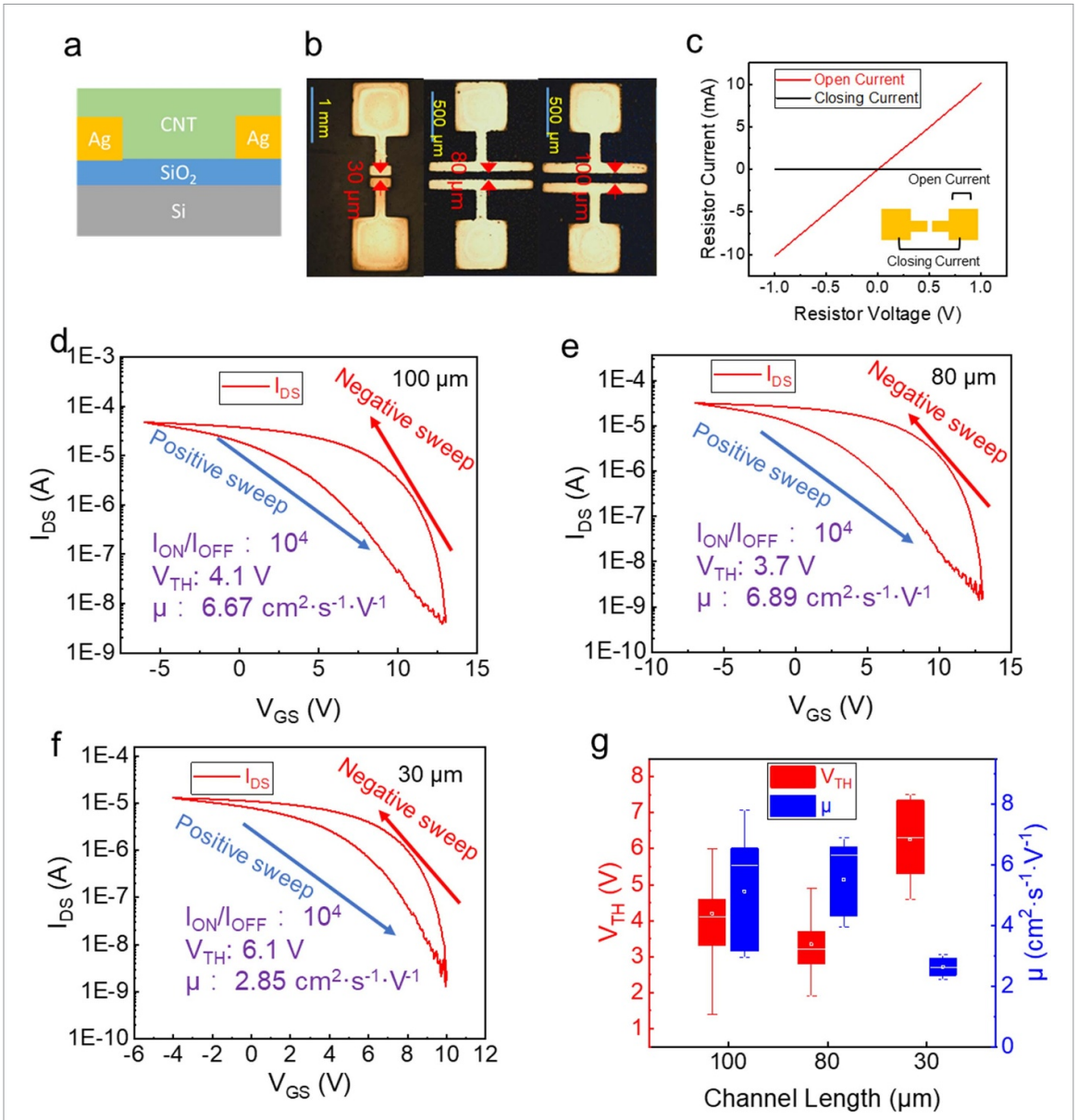

Figure 5. (a) Structure of bottom-gate bottom contact thin film transistors using carbon nanotube as the semiconductor; (b). Optical microscopes of the prepared bottom electrodes with different channel widths; (c) *I–V* curves between different regions of the electrode; ((d)–(f)) transfer *I–V* curves of the TFT with a channel width of 100 μm (d), 80 μm (e), and 30 μm (f); (g) threshold voltage and mobility of TFT devices.

positive sweep and negative sweep are within the same order of magnitude. The measured threshold voltages of 1.1–7.5 V indicate a depletion-mode operation. The devices exhibit hysteresis, which may be attributed to the influence of defects in the dielectric layer on charge and the impact of interface states. Additionally, gate current measurements indicate that leakage current ranges from 10^{-9} A to 10^{-8} A (see figure S6 in the supporting information), with some degree of fluctuation, indicating the presence of leakage current, which may be related to our device structure and manufacturing process. These transistor devices are fabricated using a fully printed method. In the channel definition, instead of lithography, a needle-tip scribing method is employed, which leads to an increase in off-state current. However, the electrodes we fabricated have undergone multiple *I–V* tests (as shown in figure 5(c)), with their off-state current as low as 10^{-12} A. This indicates that we can obtain clean channels free of silver ink residues, demonstrating that the printing process can be perfectly implemented. This does not meet the stringent requirements for leakage current in low-power logic circuit applications. However, from the perspective of certain sensor applications with relatively relaxed power consumption requirements, this leakage current is within an acceptable range.

3. Conclusion

In this work, we report the use of NBE derivative-fluorinated resin and perfluoropolyether 507 A composite films as surface wettability tuning materials for printing electronics. Leveraging the performance of low sliding angles and differences in surface energy, inks can spontaneously form patterns. The advantages of this process include simple equipment, large flexible areas, high resolution, and pattern printing achievable through blade coating. By spin-coating a layer of modified perfluoropolyether onto NBE-fluorinated resin in a two-step process, a composite film with a WCA of 113° and a water sliding angle of 47° was formed. The composite film exhibits a larger WCA, and a lower sliding angle compared to single-layer NBE films. Under irradiation with 254 nm UV light, the polymer film becomes hydrophilic, with a WCA as low as 4°. The contrast in WCA between hydrophobic and hydrophilic regions is more than 50°, and the hydrophobic regions maintain low sliding angle performance, which is conducive to the separation and migration of conductive inks, making it suitable for precision printed circuits, and further enhancing the printing resolution compared to single-layer NBE films. Additionally, we have applied this technology in TFT technology, proving that the additional pre-structuring steps have no negative impact on device performance.

4. Experimental

4.1. Materials

The photoinitiator phenyl bis(2,4,6-trimethylbenzoyl) phosphine oxide (BAPO), pentaerythritol tetra(3-mercaptopropionate) (PETMP), and 2-nitro-p-xylylene glycol were procured from TCL-SCT. Fluorolink MD®700 was supplied by Foshan Zhaojing Environmental Protection Technology Co., Ltd Isobornyl acrylate was acquired from J&K Scientific, whereas acryloyl chloride was provided by Adamas-beta. Reagents from Bruno Bock Thiochemicals (Germany) were utilized as received. The modified perfluoropolyether (507 A) was sourced from SINO-FLUORINE Technologies Co., Ltd All chemical reagents were employed without further purification. (2-Nitro-1,4-phenylene)bis(methylene)diacrylate (acrylate-NBE) was synthesized following the literature-reported procedure (see detailed characterization in figure S1 of the supporting information) [24].

4.2. Preparation and hydrophobic properties of composite films

The resin formulation was prepared following the procedure reported by Shui *et al* [11]: acrylate-NBE and isobornyl acrylate were mixed at an equimolar ratio of 37.5 mol%, with 1 wt% fluorinated methacrylate (Fluorolink MD®700) added. The thiol content in the mixture was 25 mol%, and 2.5 wt% phenyl bis(2,4,6-trimethylbenzoyl)phosphine oxide (BAPO) was used as the photoinitiator. The resin components were dissolved in chloroform and stirred in an ultrasonic bath for 10 min. For sample preparation, the solution was spin-coated onto a clean glass substrate, followed by visible light irradiation (HSPY-60-05 LED curing lamp, 230 mW cm^{-2}, 420 nm) to generate a hydrophobic film.

Subsequently, a layer of modified perfluoropolyether (507 A, supplied by Sino-Fluorine Technologies Co. Ltd) was spin-coated onto the cured film, with its thickness regulated by the spin-coating speed. The composite film was obtained after annealing and curing, and its wettability was characterized using an automatic tilting contact angle meter (SDC-350D). Specifically, static contact angles (2 μl droplet volume) and sliding angles (8 μl droplet volume) of water on the film surface were measured.

4.3. Spontaneous patterning of complex electronic circuits

The cured samples underwent selective UV irradiation (UVLED-3535, 25 mW·cm^{-2} at 254 nm) for 3000 s in air, with pattern transfer achieved via a contact photomask. For conductive patterning, Ag ink (SicrysTMI40DM-106) was employed, and the Ag nanoparticle ink was applied onto the hydrophilic/hydrophobic patterned substrate using a standard blade-coating technique, enabling spontaneous formation of conductive traces. The blade traversed the substrate at a rate of 1 millimeter per second. Post ink self-assembly, the complex electronic circuits were first air-dried under ambient conditions and subsequently sintered at 300 °C for 30 min.

4.4. CNT transistor fabrication and test

Preparation of source and drain electrodes:
On a clean Si/50 nm SiO_x substrate, the acrylate-NBE solution was spin-coated and irradiated with visible light (HSPY-60-05 LED curing lamp, 230 mW · cm^2, 420 nm) to generate a hydrophobic film. Then, a layer of 507 A (provided by Sino-Fluorine Technologies Co., Ltd) was spin-coated on the cured sample at 4000 rpm. After annealing, the sample was exposed to UV light (UVLED-3535; 25 mW · cm^2; 254 nm) and selectively irradiated through a contact photomask for 3000 s in air. Subsequently, conductive patterns were formed using Ag ink (SicrysTMI40DM-106) with a water: DGME ratio of 1:5. The scraper moved at a speed of 1 mm/s, and after ink self-assembly, silver electrodes with channel widths of 30/80/100 μm were formed. The electrodes were dried directly under ambient conditions and then sintered at 300 °C for 30 min. Using the same method, electrode samples

with a channel width of 7 μm were prepared on a clean Si/100 nm SiO_x substrate.

Semiconductor single-walled CNT solution preparation:
20 mg of Arc SWCNTs and 20 mg of poly [9-(1-octylphenyl)-9 h-carbazole2,7-diyl (PCz) polymer were weighed and dissolved in 20 ml of toluene solution. The solution was sonicated for 30 min using an 800 W cell pulverizer (Sonics VCX500) at an amplitude of 40%, and the temperature was controlled at 8 °C during sonication using a low-temperature thermostatic reaction bath to eliminate the heat generated during the sonication process. The SWCNT solution was then centrifuged at high speed for 1 h at 45 000 g. The high-purity s-SWCNTs solution was obtained by collecting 80% of the supernatant.

Deposition of s-SWCNTs films:
Silicon wafers with electrode devices were blown with N_2 gun to remove surface impurities, after low temperature plasma surface treatment instrument. (gas O_2, 100 W power, reaction time 90 s). The s-SWCNTs solution was diluted 50 times with toluene, poured into the ultra-flat surface petri dish, and put into the treated silicon wafers with electrode devices, and deposited naturally for 1 h. Remove the silicon wafers with electrode devices and put them into toluene solution, soak and clean them for 10 min, and then blow dry them with nitrogen gas for spare use.

The CNT TFT devices were characterized using a probe stage combined with a semiconductor analyzer (Keithley 4200).

Data availability statement

All data that support the findings of this study are included within the article (and any supplementary files).

Acknowledgment

The authors would like to acknowledge the financial support from Guangdong Basic and Applied Basic Research Foundation (Grant No. 2020B1515120059), the Postdoctoral Programm of Guangdong Institute of Semiconductor Micro-Nano Manufacturing Technology (2022BA09000), and the National Natural Science Foundation of China (Grant No. 22372193).

ORCID iDs

Hui Xu 0009-0006-0801-7597
Yabin Zhang 0009-0005-4452-2446
Jian Lin 0000-0002-3037-7023
Song Qiu 0000-0001-6965-4940
Chang-Qi Ma 0000-0002-9293-5027

References

[1] Wu W 2022 *Printed Electronics Technologies* (Royal Society of Chemistry) (https://doi.org/10.1039/9781788019699-FP007)
[2] Zhou Y, Qamar O A, Byoung Hwang G, Knapp C, Li G, Lubineau G and Tai Y 2024 Next-generation tattoo-like-electronics with promising fabrication and wider application scenarios *Chem. Eng. J.* **500** 157336
[3] Liu Y, Zhu H, Xing L, Bu Q, Ren D and Sun B 2023 Recent advances in inkjet-printing technologies for flexible/wearable electronics *Nanoscale* **15** 6025–51
[4] Liu Y *et al* 2024 Fully inkjet-printed Ag_2Se flexible thermoelectric devices for sustainable power generation *Nat. Commun.* **15** 2141
[5] Kim Y Y, Yang T-Y, Suhonen R, Välimäki M, Maaninen T, Kemppainen A, Jeon N J and Seo J 2019 Gravure-printed flexible perovskite solar cells: toward roll-to-roll manufacturing *Adv. Sci.* **6** 1802094
[6] Yang L, Lopes I C and Vadgama P 2023 Self-cleaning sensors based on thermoresponsive polymeric film modified screen-printed platinum electrodes *Chem. Eng. J.* **474** 145932
[7] Xiong K, Hou L, Wu M, Huo Y, Mo W, Yuan Y, Sun S, Xu W and Wang E 2015 From spin coating to doctor blading: a systematic study on the photovoltaic performance of an isoindigo-based polymer *Solar Energy Mater. Solar Cells* **132** 252–9
[8] Oberdick S D and Zabow G 2020 Patterned surface energy in elastomeric molds as a generalized approach to polymer particle fabrication *ACS Appl. Polym. Mater.* **2** 846–52
[9] Rossegger E, Hennen D, Griesser T, Roppolo I and Schlögl S 2019 Directed motion of water droplets on multi-gradient photopolymer surfaces *Polym. Chem.* **10** 1882–93
[10] Li L, Li W, Sun Q, Liu X, Jiu J, Tenjimbayashi M, Kanehara M, Nakayama T and Minari T J S 2021 Dual surface architectonics for directed self-assembly of ultrahigh-resolution electronics *Small* **17** 2101754
[11] Shui K *et al* 2023 UV-converted heterogeneous wettability surface for the realization of printed micro-scale conductive circuits *Flexi. Printed Electron.* **8** 035019
[12] Feng R, Song F, Zhang Y-D, Wang X-L and Wang Y-Z 2022 A confined-etching strategy for intrinsic anisotropic surface wetting patterning *Nat. Commun.* **13** 3078
[13] Naderi P, Sheuten B R, Amirfazli A and Grau G 2023 Inkjet printing on hydrophobic surfaces: controlled pattern formation using sequential drying *J. Chem. Phys.* **159** 024712
[14] Docherty M J, Naderi P, Grau G, Sefiane K and Amirfazli A 2024 Inkjet printing on hydrophobic surface: practical implementation of stacked coin strategy *Adv. Eng. Mater.* **26** 2400237
[15] Hadzik J *et al* 2023 An experimental anodized and low-pressure oxygen plasma-treated titanium dental implant surface—preliminary report *Int. J. Mol. Sci.* **24** 3603
[16] Zou X P, Kang E T, Neoh K G, Cui C Q and Lim T B 2001 Surface modification of poly(tetrafluoroethylene) films by plasma polymerization of glycidyl methacrylate for adhesion enhancement with evaporated copper *Polymer* **42** 6409–18
[17] Pierre A, Sadeghi M, Payne M M, Facchetti A, Anthony J E and Arias A C J A M 2014 All-printed flexible organic transistors enabled by surface tension-guided blade coating *Adv. Mater.* **26** 5722–7
[18] Zhu Z and Kelley M J 2004 Poly(ethylene terephthalate) surface modification by deep UV (172 nm) irradiation *Appl. Surf. Sci.* **236** 416–25
[19] Liu X, Kanehara M, Liu C, Sakamoto K, Yasuda T, Takeya J and Minari T J A M 2016 High-resolution electronics: spontaneous patterning of high-resolution electronics via parallel vacuum ultraviolet *Adv. Mater.* **28** 6768
[20] Liu X, Kanehara M, Liu C, Sakamoto K, Yasuda T, Takeya J and Minari T J A M 2016 Spontaneous patterning of high-resolution electronics via parallel vacuum ultraviolet *Adv. Mater.* **28** 6568–73

[21] Kaneko S, Yamamoto Y, Wada K, Kumagai G, Harada Y, Yamauchi R and Ishibashi Y 2020 Ultraviolet irradiation improves the hydrophilicity and osteo-conduction of hydroxyapatite *J. Orthop. Surg. Res.* **15** 425
[22] Huang Z and Wang H 2023 Turning danger into opportunity: ultraviolet (UV) irradiation-surface reconstruction effect of hydrophilic plastics and its application in plastic flotation separation *J. Environ. Chem. Eng.* **11** 110659
[23] Liu Q *et al* 2024 Optimization of durable superhydrophobic wood with superstrong ultraviolet resistance and chemical stability *Chem. Eng. J.* **480** 148164
[24] Rossegger E, Nees D, Turisser S, Radl S, Griesser T and Schlögl S 2020 Photo-switching of surface wettability on micropatterned photopolymers for fast transport of water droplets over a long-distance *Polym. Chem.* **11** 3125–35
[25] Littlejohn D and Chang S-G 1995 An XPS study of nitrogen-sulfur compounds *J. Electron Spectrosc. Relat. Phenom.* **71** 47–50
[26] Tothadi S, Shaikh T R, Gupta S, Dandela R, Vinod C P and Nangia A K 2021 Can we identify the salt–cocrystal continuum state using XPS? *Cryst. Growth Des.* **21** 735–47
[27] Mostegel F H *et al* 2015 Versatile thiol-based reactions for micrometer- and nanometer-scale photopatterning of polymers and biomolecules *J. Mat. Chem. B* **3** 4431–8
[28] Bhatia S K, Hickman J J and Ligler F S 1992 New approach to producing patterned biomolecular assemblies *J. Am. Chem. Soc.* **114** 4432–3
[29] Radl S V, Schipfer C, Kaiser S, Moser A, Kaynak B, Kern W and Schlögl S 2017 Photo-responsive thiol–ene networks for the design of switchable polymer patterns *Polym. Chem.* **8** 1562–72